ARTICLE TEMPLATE

Geophysical Imaging of Subsurface Structures with Least Squares Estimates

Hank Hetrick[a] and Jodi Mead[b]

[a]Department of Geosciences, Boise State University, 1910 University Dr., Boise, Idaho 83702; [b]Department of Mathematics, Boise State University, 1910 University Dr., Boise, Idaho 83702

ARTICLE HISTORY
Compiled December 31, 2017

ABSTRACT
Electrical resistivity tomography (ERT) is a useful tool for subsurface imaging. However, the resulting nonlinear inverse problem is severely under-determined. Smoothness constraints are commonly implemented with least squares to make the problem solvable, but the constraints limit the ability to produce discontinuities in the model parameters. In practice, sharp delineations have been recovered with these constraints by applying appropriate weights or covariance matrices which relax the constraint at different regions [10, 14, 15, 19, 26]. For example in medical imaging, anatomical information has been included in electrical impedance tomography (EIT) through matrix valued fields [3, 4, 16]. More closely related to this work, prior structural information was added to ERT inversion through matrix valued fields [12]. In this work, we analyze the binary matrix that relaxes the smoothness constraint in locations where there is a known boundary. Analysis of the recovered parameters using this matrix gives insight as to the type of heterogeneities that can be recovered. We conclude that it is more effective to include structural information with 1^{st} and 2^{nd} order derivative constraints than with initial parameter estimates. In addition, we show that the 1^{st} derivative constraint produces models with piecewise constant variability, while a 2^{nd} derivative will yield linear variability. These conclusions are verified on synthetic ERT inversions in seven different subsurface structures.

KEYWORDS
Electrical Resistivity Tomography; Nonlinear Inverse Problems; Discontinuous Inversions; Regularization; MSC 86A22

AMS CLASSIFICATION
86A22

1. Introduction

Most inverse methods in geophysics require regularization, especially in the subsurface where direct observations are expensive and unavailable. Typically smoothing constraints are implemented in a least squares inversion [7, 9]. They are useful for producing general trends interpretable at large spatial scales, and have proven to be especially useful when temporal data is available to compare changes in the subsurface with time.

Hank Hetrick. Email: hankhetrick@u.boisestate.edu Fax: 208 426-1356
Jodi Mead. Email:jmead@boisestate.edu Tel.: 208 426-2432 Fax: 208 426-1356 This work was supported by NSF grant DMS 1418714

Most geophysical studies have a known discontinuous boundary present in the subsurface such as permafrost, bedrock, or the water table. The implementation of smoothness constraints is not ideal because they prevent the ability to produce model parameters with discontinuities. For example, an accurate, quantitative analysis of soil moisture requires inverse methods that allow sharp changes in soil properties. For this reason, the conventional approach for inverse problems with sharp discontinuities is to avoid smoothing operators [2].

Numerical results in Section 4 focus on imaging subsurface structures using electrical resistivity tomography (ERT). There have been some studies that promote and implement the use of discontinuities in a least squares ERT inversion in a variety of different ways. This includes semivariogram constraints [14, 15], joint inversion [11], covariance matrices [26], and active Lagrange Parameters [17]. In some cases, the location of the discontinuity is incorporated into the model parameters themselves [30].

The most general approach of incorporating discontinuities is by relaxing the smoothness constraint [12]. This is done in [10] where information about a discontinuity is derived from ground penetrating radar (GPR). The information has also come from well data [15], or known man-made structures in the subsurface [28]. However, an investigation of how to add discontinuities through a smoothness constraint, and its consequences, has not been provided. Therefore, in this work we define the regularization operator that relaxes the constraint in two dimensions and determine that the 1^{st} and 2^{nd} derivative regularization operators effectively capture discontinuities. This result is counter to most regularization methods that use 1^{st} and 2^{nd} derivative operators to produce smooth solutions [2].

Similar to ERT, electrical impedance tomography (EIT) uses low frequencies to measure resistivity and typically results in an ill-posed inverse problem. EIT is often used in medical imaging and can be considered more general than ERT because the imaginary component is more dominant and the frequency dependence on conductivity can be utilized. Recent work on imaging conductivity anomalies from boundary measurements can be found in [3, 4]. In that work the anomalies and frequency dependence of their conductivities were used to significantly improve their imaging in a heterogeneous environment.

Including prior information involving anatomical structure in EIT medical imaging was introduced in [16]. This is analogous to including boundary information in the Earth's subsurface. Similar to this work, in [16] the prior information is incorporated in a Tikhonov regularization term with a matrix valued field. They give results with both a 0^{th} and 1^{st} derivative operators. In Section 2 we explain that prior boundary information should be included with either a 1^{st} or 2^{nd} derivative operator, and not with a 0^{th}, i.e. an initial parameter estimate. This is justified with a simple mathematical explanation, where we also explain that the recovered variability in the heterogeneous environment will be constant with a 1^{st} derivative constraint, and linear with 2^{nd} derivative constraint.

We begin in Section 2 by explaining the effect of typical smoothness constrains in an inversion and how a least squares regularization can allow for discontinuities. We illustrate these points with a simple example. In Section 3 we discuss the assumptions that are made when relaxing the smoothness constraint to produce discontinuities and expand the implementation into a two dimensional problem with Occam's method. Our synthetic results in Section 4 include ERT simulations on seven different types of true model parameters, and compare the performances of the derivative operators as constraints.

2. Discontinuous Inversions

2.1. *The Constraint*

Smooth model inversion can be viewed as constrained optimization, i.e.

$$min(\phi_d(\mathbf{m})), \quad s.t. \;\; ||\mathbf{L}_p(\mathbf{m} - \mathbf{m}_{ref})||_2^2 \leq \delta$$

where

$$\phi_d(\mathbf{m}) = ||F[\mathbf{m}] - \mathbf{d}||_2^2.$$

The value of ϕ_d is the data residual, $\mathbf{m}$ contains the unknown model parameters, $F[\mathbf{m}]$ is the mathematical model, and $\mathbf{d}$ are observational data. The constraint term contains the p^{th} derivative operator $\mathbf{L}_p$, and $\mathbf{m}_{ref}$ is a reference model or initial parameter estimate. The goal of the constraint term in regularization is to stabilize the inversion problem such that small perturbations in the data yields small perturbations in the inverted model. The constraint term can also be viewed as adding prior information, where the type of constraint should reflect something already known about the true model. By viewing the regularization terms as constraints containing prior information, we develop a detailed understanding of producing discontinuous parameters with p^{th} derivative constraints.

When the zeroth derivative is used, the derivative operator becomes the identity matrix:

$$\mathbf{L}_0 = \mathbf{I}.$$

With this approach, the reference model $\mathbf{m}_{ref}$ is used as the primary constraint, i.e.:

$$||\mathbf{m} - \mathbf{m}_{ref}||_2^2 \leq \delta$$

is prior information on the model parameters. If the reference model is a good estimate, or if the estimate is correctly weighted, then the inversion yields acceptable results. However, good reference model parameters require both the location of the discontinuity, as well as estimates of the model parameters. If the location of the discontinuities are known, it was shown in [20] that appropriate weights within each subregion can be found with multiple χ^2 tests. The objectives here include defining how to incorporate known discontinuities in least squares estimates, and identifying the proper use of derivative operators $\mathbf{L}_p$ that avoids the need to give good model parameter estimates.

If one seeks to provide detailed reference model parameters through the use of the $\mathbf{L}_0$ constraint, it takes away the purpose of the inversion to find the model parameters. Therefore, we focus on constraining the 1st and 2nd derivatives through $\mathbf{L}_1$ and $\mathbf{L}_2$ where the reference model parameters are typically a zero vector. Less information is needed with the $\mathbf{L}_1$ and $\mathbf{L}_2$ operators because the meaning of the constraint drastically changes from when it was constrained with $\mathbf{L}_0$. The $\mathbf{L}_1$ and $\mathbf{L}_2$ constraints do not require specific values for the parameter estimates, only that they should be smooth. We take this simpler smooth parameters constraint and show how it can be used as a constraint that specifies the discontinuities.

2.2. *The Regularization Operator*

Appropriate weights or error covariance matrices for the constraint allow the constraint to be relaxed in different regions. If the location of the discontinuity is known it can be identified with a binary matrix, or regularization operator, which we notate as $\mathbf{R}$

$$\mathbf{R} = diag(r_1, r_2, ..., r_n), \quad r_i = 0 \text{ or } 1, \tag{1}$$

where n is the number of rows in $\mathbf{L}_p$, and typically the number of parameters. This operator $\mathbf{R}$ is incorporated in the inversion as follows

$$\phi(\mathbf{m}) = ||\mathbf{W}_d(\mathbf{d} - \mathbf{F}[\mathbf{m}])||_2^2 + \alpha^2||\mathbf{R}\mathbf{L}_p\mathbf{m}||_2^2, \tag{2}$$

where $\mathbf{W}_d$ is a weight on the data error, representing the error covariance matrix. When there is a sharp discontinuity, $r_i = 0$ is chosen at that spatial location indicating that there is no smoothness. A value of one is assigned to all other values of r_i. The result of applying $\mathbf{R}$ is that only data inform the value of the parameters at the specified discontinuity.

This approach is similar to the regularization matrix R used in [1]. The difference in the discussion in [1] and here is that we do not assume R^TR represents the prior inverse error covariance matrix. We will show results minimizing (2) when $\mathbf{L}_p = \mathbf{I}$, however, including $\mathbf{R}$ with that constraint is redundant in our definition of $\mathbf{R}$ because $\mathbf{m}_{ref}$ already contains the boundary information. In addition, the weight on the boundary information contained in $\mathbf{m}_{ref}$ (which reflects its error covariance) is not treated as an input to the algorithm here, rather it is determined in the regularization parameter(s) selection method. Results in Section 4 use the χ^2 method [22] to find this weight. We find that assuming the error covariance for the initial parameter estimate is known, and can be inputted into the algorithm, is not realistic. Alternatively, we find that knowledge of the location of the boundary can be reliably inferred from other data, and that is all that is required to define $\mathbf{R}$.

For example, in the one-dimensional case consider six model parameters. Applying the first derivate operator $\mathbf{L}_1$ results in the constraint

$$\mathbf{L}_1\mathbf{m} = \frac{1}{\Delta x}\begin{pmatrix} m_2 - m_1 \\ m_3 - m_2 \\ m_4 - m_3 \\ m_5 - m_4 \\ m_6 - m_5 \\ 0 \end{pmatrix}.$$

If a sharp transition occurs in-between m_2 and m_3, and m_4 and m_5 then

$$\mathbf{R} = diag(1, 0, 1, 0, 1, 1)$$

so that the total product yields:

$$\mathbf{RL}_1\mathbf{m} = \frac{1}{\Delta x}\begin{pmatrix} m_2 - m_1 \\ 0 \\ m_4 - m_3 \\ 0 \\ m_6 - m_5 \\ 0 \end{pmatrix}.$$

In this case the 1st derivative constraint is applied everywhere except along the transition between m_2 and m_3 as well as a second discontinuity between m_4 and m_5. When the regularization matrix is included with the constraint term, the result in an array of inverted parameters with discontinuities delineating between piecewise smooth regions.

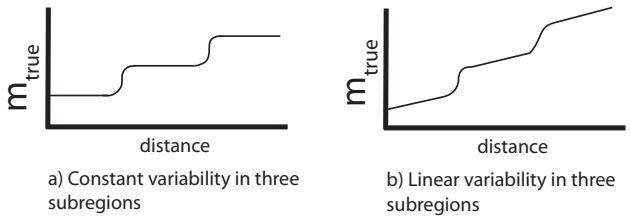

Figure 1. True parameters for the simple layered example.

2.3. *Derivative Constraints*

Here we study the effects of 1^{st} and 2^{nd} derivative constraints with or without the incorporation of the regularization operator $\mathbf{R}$ on a canonical three layered subsurface model. It is assumed that there is a large weight on the constraint term so that we can understand the constraint's effect on the inversion. We denote the inverted parameters by:

$$\begin{aligned} \mathbf{m}_{\mathbf{RL}_p} &= argmin(\phi(\mathbf{m})) \quad for \;\; \mathbf{R} \neq \mathbf{I} \\ \mathbf{m}_{\mathbf{L}_p} &= argmin(\phi(\mathbf{m})) \quad for \;\; \mathbf{R} = \mathbf{I} \end{aligned}$$

Figure 1(a) gives an idealized example of a true model with piecewise constant variability in the subregions, while Figure 1(b) reflects linear variability in the subregions.

When the constraint term is implemented with a 0^{th} derivative operator and a reference model $\mathbf{m}_{ref}$, a large weight on the constraint implies that the inverted result $\mathbf{m}_{L_0}$ is going to be the same as the provided reference model. However, if the regularization operator is included into the constraint term, then the inverted result $\mathbf{m}_{RL_0}$ will not be the reference model at the boundaries. This is because the regularization operator completely removes any influence of the reference model on the inverted model parameters at the specified boundary. The values in such regions near the boundary are solely dependent on the observational data, including any noise that may be present. This is not advantageous since it nullifies the reference model constraint at the boundaries and hence we do not recommend using the $\mathbf{L}_0$ constraint with the regularization operator $\mathbf{R}$.

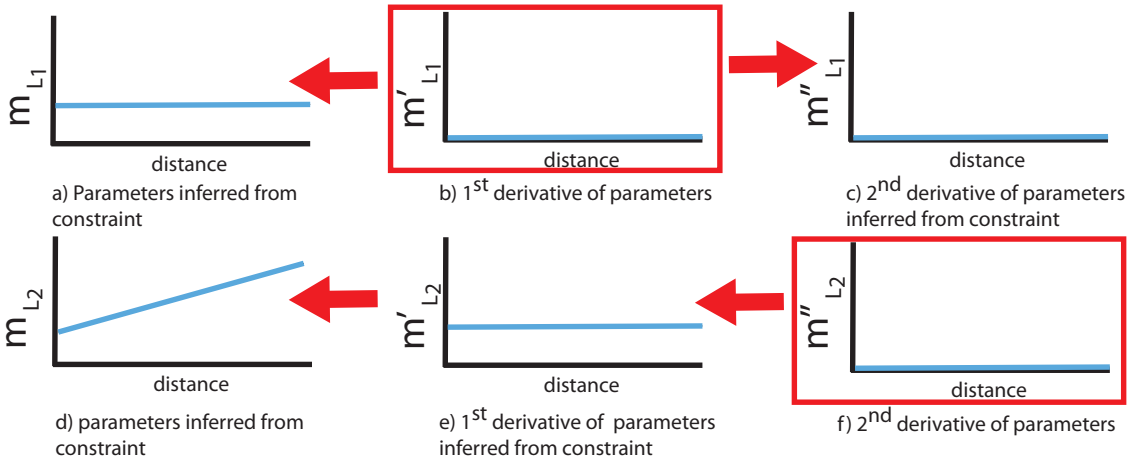

Figure 2. Inverted parameters and their derivatives in piecewise constant variability simple example, Figure 1(a). $\mathbf{L}_1$ enforced exactly in (a)-(c), $\mathbf{L}_2$ constraint enforced exactly in (d)-(f). Red boxes indicate exact constraint used for inversion.

The rows in each of Figures 2-5 show the idealized inverted parameters in the 1^{st} column, along with their 1^{st} and 2^{nd} derivatives in the 2^{nd} and 3^{rd} columns, respectively. Figures 2 and 4 give idealized inverted results with the standard smoothness constraints $\mathbf{L}_1\mathbf{m}$ and $\mathbf{L}_2\mathbf{m}$ while the effect of the regularization operator through discontinuous smoothness constraints $\mathbf{RL}_1\mathbf{m}$ and $\mathbf{RL}_2\mathbf{m}$ is shown in Figures 3 and 5. When $\mathbf{R} \neq \mathbf{I}$ is applied as the constraint, $\mathbf{m}_{RL_1}$ and $\mathbf{m}_{RL_2}$ only fit data at the specified discontinuities, and this is indicated by the open circles in Figures 3 and 5.

The first columns in Figures 2 and 4 show how inverted results with 1^{st} and 2^{nd} derivative constraints merely provide a constant or linear average of parameter estimates, respectively. Alternatively, the first columns in Figures 3 and 5 show how the regularization operator applied to both 1^{st} and 2^{nd} derivative constraints can yield inverted parameters that both include the presence of a boundary as well as reflect constant or linear variability within each subregion.

It is important to emphasize that the choice of using the 1^{st} or 2^{nd} derivative as the constraint term rests on two factors: 1) the amount (or lack) of variability within each region separated by the discontinuities, and 2) the degree of sensitivity that the observational data have on each of these regions. Due to the dependence of the sensitivity of the data to the model parameters, no theoretical absolute dictates which constraint would perform consistently better when applied to a problem where the variability between the model parameters do not vary. Clearly the 1^{st} derivative would be a good choice, however, the 2^{nd} derivative could also yield the same results. This performance would be purely dependent on the spatial sensitivity between the observations and each region in the model parameters. With greater sensitivity, the 2^{nd} derivative constraint would perform just as good as the 1^{st} derivative constraint for model parameters with discontinuities separating regions that have no variability. In this case, the 2^{nd} derivative has the potential to provide optimal results in either constant or linear variability subregions. Therefore, through this simple example we have not only explained the effect of the regularization operator $\mathbf{R}$, but have also justified why most geophysical applications find success with the 2^{nd} derivative constraint. We verify these conclusions in an ERT synthetic inversion in Section 4.

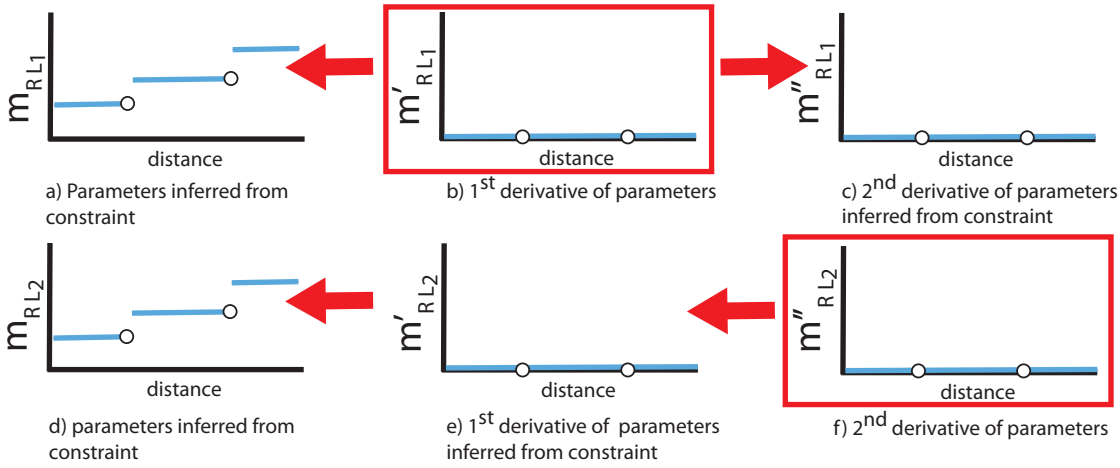

Figure 3. Inverted parameters and their derivatives in piecewise constant variability simple example, Figure 1(a). $\mathbf{RL}_1$ enforced exactly in (a)-(c), $\mathbf{RL}_2$ constraint enforced exactly in (d)-(f). Red boxes indicate exact constraint used for inversion.

3. Implementation of the Regularization Operator

3.1. *Assumptions*

The first and foremost assumption made in this work is that the location of the discontinuities is known. In the case of geophysical investigations, this would imply that there is another dataset that provides the location of subsurface boundaries. The second assumption is that the discontinuity is sharp such that the distance of the transition that occurs between each region is small relative to the spatial resolution of the model parameters. A good example occurs frequently with electrical resistivity tomography, wherein the spatial resolution of the model parameters are on the order of the electrode separation. This distance is typically much greater than the vertical transition across the water table, which is typically on the order of centimeters, so that the transition of electrical properties across this boundary is effectively discontinuous relative to the discretization of the inverted resistivity profiles. The third assumption is that the observational data must have sensitivity to each region that the discontinuity delineates. If the data is not sensitive to any regions separated by a boundary, then the data is not likely sensitive to the boundary itself, and implementing a regularization operator into the inversion process will not provide a significant benefit to the problem.

3.2. *The Two-Dimensional Problem*

Our synthetic results include inversions of electrical resistivity tomography for a variety of resistivity distributions within the subsurface. The models in these problems are two dimensional and Occam's method is used to solve the nonlinear optimization problem with cost function:

$$\phi(\mathbf{m}) = ||\mathbf{W}_d(\mathbf{d} - \mathbf{F}[\mathbf{m}])||_2^2 + \alpha^2[||\mathbf{L}_{px}\mathbf{m}||_2^2 + ||\mathbf{L}_{pz}\mathbf{m}||_2^2]$$

where $\mathbf{L}_{px}$ and $\mathbf{L}_{pz}$ are derivative operators in the x and z spatial directions. In two dimensions, there are two regularization matrices $\mathbf{R}_x$ and $\mathbf{R}_z$ that identify boundaries

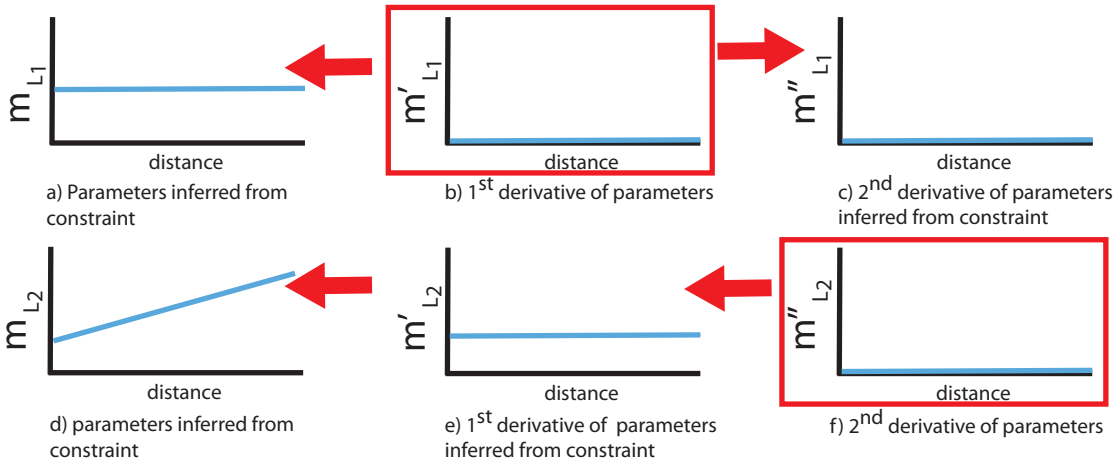

Figure 4. Inverted parameters and their derivatives in linear variability simple example, Figure 1(a). $\mathbf{L}_1$ enforced exactly in (a)-(c), $\mathbf{L}_2$ constraint enforced exactly in (d)-(f). Red boxes indicate exact constraint used for inversion.

in each direction. The cost function with boundary information becomes

$$\phi(\mathbf{m}) = ||\mathbf{W}_d(\mathbf{d} - \mathbf{F}[\mathbf{m}])||_2^2 + \alpha^2[||\mathbf{R}_x\mathbf{L}_{px}\mathbf{m}||_2^2 + ||\mathbf{R}_z\mathbf{L}_{pz}\mathbf{m}||_2^2].$$

3.3. *Occam's Method*

Occam's method is a commonly used technique in geophysics for nonlinear inversions [7], [9]. It requires an initial iterate $\mathbf{m}_{(0)}$ so that Taylor's theorem gives a local linear approximation of $\mathbf{F}[\mathbf{m}]$. The objective function becomes

$$\begin{aligned}\phi_k(\mathbf{m}_{(k+1)}) &= \phi_{d(k)} + \alpha^2[\phi_{mx(k)} + \phi_{mz(k)}] \\ &= ||\mathbf{W}_d(\hat{\mathbf{d}}_{(k)} - \mathbf{J}_{(k)}\mathbf{m}_{(k+1)})||_2^2 + \alpha^2[||\mathbf{R}_x\mathbf{L}_{px}(\mathbf{m}_{(k+1)} - \mathbf{m}_{ref})||_2^2 \\ &\quad + ||\mathbf{R}_x\mathbf{L}_{pz}(\mathbf{m}_{(k+1)} - \mathbf{m}_{ref})||_2^2]\end{aligned}$$

with $\mathbf{J}_{(k)}$ the Jacobian of F evaluated at $\mathbf{m}_{(k)}$ and

$$\hat{\mathbf{d}}_k = \mathbf{d} - \mathbf{F}[\mathbf{m}_{(k)}] + \mathbf{J}_{(k)}\mathbf{m}_{(k)}.$$

At each iterate, the minimum of the linear cost function occurs at:

$$\begin{aligned}\mathbf{m}_{(k+1)} &= [\alpha^2(\mathbf{L}_{px}^T\mathbf{R}_x^T\mathbf{R}_x\mathbf{L}_{px} + \mathbf{L}_{pz}^T\mathbf{R}_z^T\mathbf{R}_z\mathbf{L}_{pz}) + \mathbf{J}_{(k)}^T\mathbf{W}_d^T\mathbf{W}_d\mathbf{J}_{(k)}]^{-1}[\mathbf{J}_{(k)}^T\mathbf{W}_d^T\mathbf{W}_d\hat{\mathbf{d}}_{(k)} \\ &\quad -\alpha^2(\mathbf{L}_{px}^T\mathbf{R}_x^T\mathbf{R}_x\mathbf{L}_{px} + \mathbf{L}_{pz}^T\mathbf{R}_z^T\mathbf{R}_z\mathbf{L}_{pz})\mathbf{m}_{ref}].\end{aligned}$$

Occam's method uses the discrepancy principle in order to find the regularization parameter α, i.e. α is found so that:

$$\phi_d(\mathbf{m}_{(k+1)}) \leq \Delta.$$

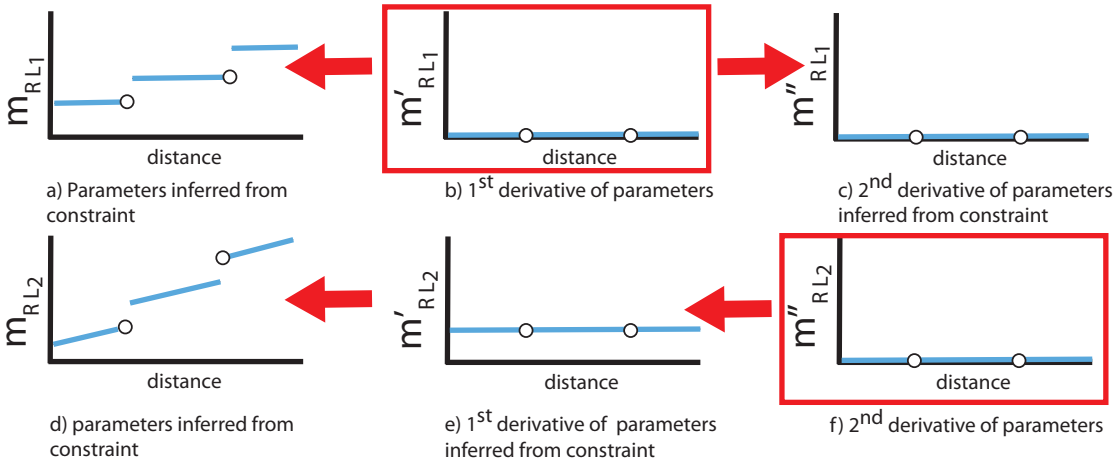

Figure 5. Inverted parameters and their derivatives in linear variability simple example, Figure 1(a). $\mathbf{RL}_1$ enforced exactly in (a)-(c), $\mathbf{RL}_2$ constraint enforced exactly in (d)-(f). Red boxes indicate exact constraint used for inversion.

The choice of Δ is often left as an open question. If the data misfit is considered as a χ^2 random variable, its mean can be used for Δ. In this case the degrees of freedom (and its mean) is $m-n$, where m is the number of data and n is the number of parameters. For $m \approx n$ this approach is not practical and the χ^2 method [21, 22] that uses the regularized residual can be used. In the χ^2 method α is found so that:

$$\phi(\mathbf{m}_{(k+1)}) \approx \bar{\chi}^2_m = m.$$

Not only does the χ^2 method give a statistical justification for the choice of α, we suggest that it is important to include this sensitivity towards the constraint when choosing the regularization parameter because it will be more sensitive to the type of constraint used within the inversion process. If a good estimate of the boundary location is properly implemented into the regularization matrix, then $||\mathbf{RL}_p\mathbf{m}_{true}||_2^2$ will be small relative to other potential estimates of the boundary contained in $\mathbf{R}$. This implies inverted results should reflect a greater weight on minimizing the regularization residual. Therefore, if the presence of a sharp boundary is known prior to data acquisition or processing but not the exact location, then a variety of boundary estimates will provide different regularization parameters, which will yield different inverted results. The inverted result with the largest regularization parameter found by the χ^2 test will indicate that the associated boundary estimate is the most probable. This will be explored in future work.

4. Numerical Results

4.1. *The Forward Model: Ohm's Law*

Electrical resistivity tomography is used to approximate two or three dimensional models of electrical resistivity within the subsurface. This geophysical method has proven to be useful for a wide variety of subsurface investigations including salt water intrusions [13, 14, 29], tracer studies [18, 24, 27, 31], and vadose zone soil moisture

analysis [5, 8, 23].

Resistivity data is acquired by distributing either a line or grid of electrodes along the surface. A pair of transmitting electrodes are used to induce a low frequency, alternating current, into the ground. A separate pair of receiver electrodes measure the potential difference elsewhere. The ratio of the injected current and the measured voltage, combined with the electrode geometry, yields the measured result known as the apparent resistivity and is given by:

$$\rho_a = \frac{2\pi\Delta V}{i}\kappa$$

where

$$\kappa = 1/(1/\Delta x_{AM} - 1/\Delta x_{AN} - 1/\Delta x_{BM} + 1/\Delta x_{BN}).$$

The variable κ is known as the geometric factor that contains all of the geometrical information of the electrodes, ΔV is the electrical potential different across the receiver electrode pair, i is the injection current, and Δx_{AN} represents the distances between the current electrodes A and B and the voltage electrodes M and N, see Figure 6. The apparent resistivity is equivalent to what would be measured for a homogeneous subsurface. These values are treated as observational data and can be inverted to yield an approximate model of the subsurface resistivity ρ.

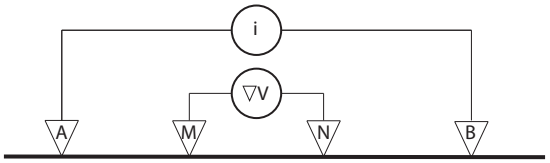

Figure 6. The Wenner-alpha electrode configuration.

The governing equation that provides the relationship between the resistivity in the subsurface and the measured apparent resistivity is Ohm's Law:

$$\nabla \cdot [\sigma(\mathbf{r})\nabla V(\mathbf{r})] = i[\delta(\mathbf{r} - \mathbf{r}_A) - \delta(\mathbf{r} - \mathbf{r}_B)]$$

where $\sigma = 1/\rho$ is the conductivity. The variables $\mathbf{r}_A$ and $\mathbf{r}_B$ represent the three dimensional (x, y, z) locations of current source electrodes A and B, respectively.

This study implements a Matlab-based 2.5D forward model developed by Adam Pidlisecky and Rosemary Knight [25], where the Fourier-transform is used in the y direction so that resistivity varies along a horizontal x and vertical z dimensions while the y dimension has constrained variability. The two-dimensional model takes the form:

$$\begin{aligned} \frac{\partial}{\partial x}[\sigma(x,z)\frac{\partial V(x,z)}{\partial x}] + \frac{\partial}{\partial z}[\sigma(x,z)\frac{\partial V(x,z)}{\partial z}] &- \lambda_y^2\sigma(x,z)V(x,z) \\ &= i\,[\delta(x - x_A) - \delta(x - x_B)] \end{aligned}$$

where λ_y represents the spatial wavenumber in the y direction, which represents the degree of variability in the y direction. This code was altered to allow conversions from electrical potential values at receiver electrode positions to apparent resistivity observations from given electrode combinations for wenner-alpha arrays [6].

The input to the forward model takes a given resistivity model

$$\mathbf{m} = \rho(x, z), \quad \mathbf{m} \in \mathbb{R}^n.$$

and with a distribution of current source locations, yields electrical potential at all locations. The associated output is converted into a set of apparent resistivity values:

$$F[\mathbf{m}] = \boldsymbol{\rho}_a, \quad F[\mathbf{m}] \in \mathbb{R}^m.$$

Therefore, the inversion of resistivity data takes measured apparent resistivities $\mathbf{d}$ as input so that

$$\mathbf{d} = F[\mathbf{m}] + \boldsymbol{\epsilon},$$

with noise $\boldsymbol{\epsilon}$. In this study, we use synthetic measurements and represent $\boldsymbol{\epsilon}$ as Gaussian noise. Even though this assumption may not be true for particular scenarios encountered in the field, it is a common assumption and will be applied in this study.

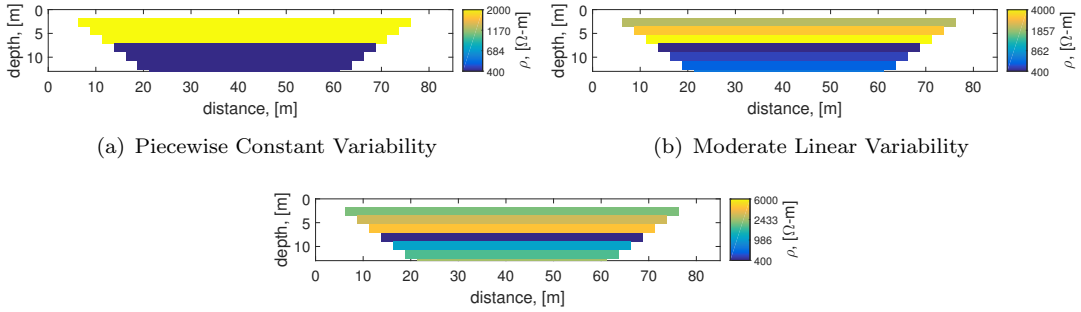

(a) Piecewise Constant Variability

(b) Moderate Linear Variability

(c) Strong Linear Variability

Figure 7. True resistivity values for a layered subsurface

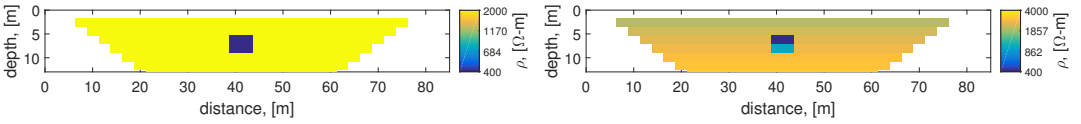

(a) Piecewise Constant Variability

(b) Moderate Linear Variability

Figure 8. True resistivity values for an anomaly model

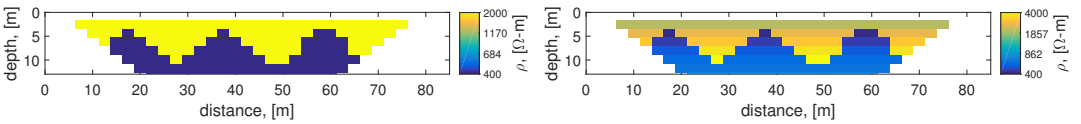

(a) Piecewise Constant Variability

(b) Moderate Linear Variability

Figure 9. True resistivity values for sinusoidal model

4.2. *Synthetic Results*

In this section, we provide inverted results from three fundamental model types: 1) two-layered models in Figure 7, 2) anomaly models in Figure 8, and 3) sinusoidal models in Figure 9. By considering both constant and linear variability in all three model types, a total of seven models were used for our synthetic analysis. These model types represent the challenge in ERT inversion with respect to the sensitivity of the observational data to 1) subregions distant from the observations, 2) subregions with small anomalies, and 3) complex subregion boundary geometry. We compare results from standard 0^{th}, 1^{st}, and 2^{nd} derivative constraint inversions to those that use discontinuous regularization operators. In each model 0.1% Gaussian noise was added to each data sample to create the synthetic observations. Four different resistivity values were estimated from each of the seven sets of synthetic data, and are denoted by $\mathbf{m_{L_0}}$, $\mathbf{m_{L_1}}$, $\mathbf{m_{L_2}}$, $\mathbf{m_{RL_0}}$, $\mathbf{m_{RL_1}}$, and $\mathbf{m_{RL_2}}$ as defined in Section 2.3.

4.2.1. Two-Layered Models

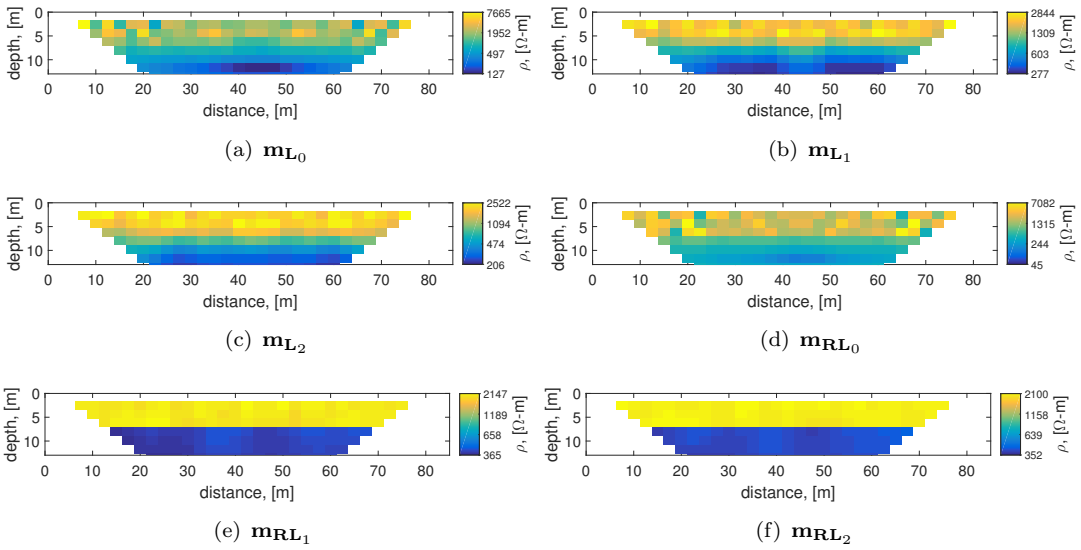

(a) $\mathbf{m_{L_0}}$ (b) $\mathbf{m_{L_1}}$

(c) $\mathbf{m_{L_2}}$ (d) $\mathbf{m_{RL_0}}$

(e) $\mathbf{m_{RL_1}}$ (f) $\mathbf{m_{RL_2}}$

Figure 10. Inverted resistivity values for a layered subsurface with piecewise constant variability

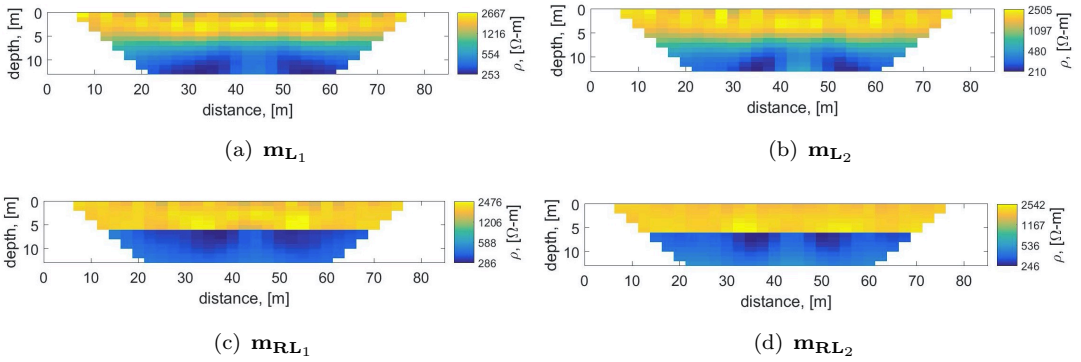

(a) $\mathbf{m_{L_1}}$ (b) $\mathbf{m_{L_2}}$

(c) $\mathbf{m_{RL_1}}$ (d) $\mathbf{m_{RL_2}}$

Figure 11. Inverted resistivity values for a layered subsurface with piecewise constant variability with data and inversion on different grids.

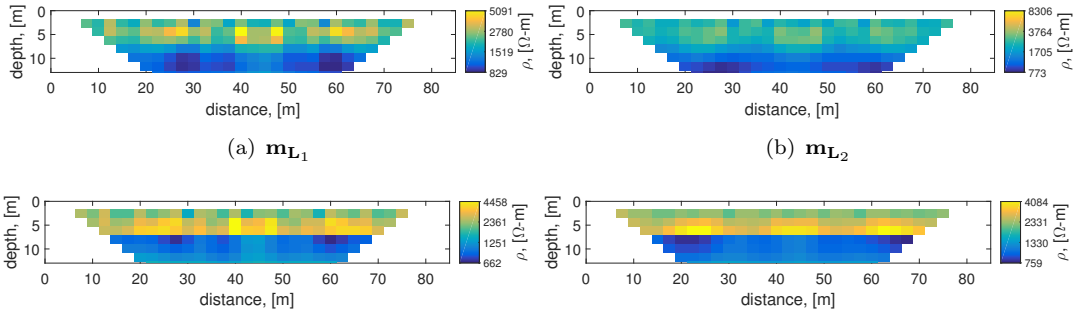

(a) $\mathbf{m_{L_1}}$ (b) $\mathbf{m_{L_2}}$

(c) $\mathbf{m_{RL_1}}$ (d) $\mathbf{m_{RL_2}}$

Figure 12. Inverted resistivity values for a layered subsurface with strong linear variability

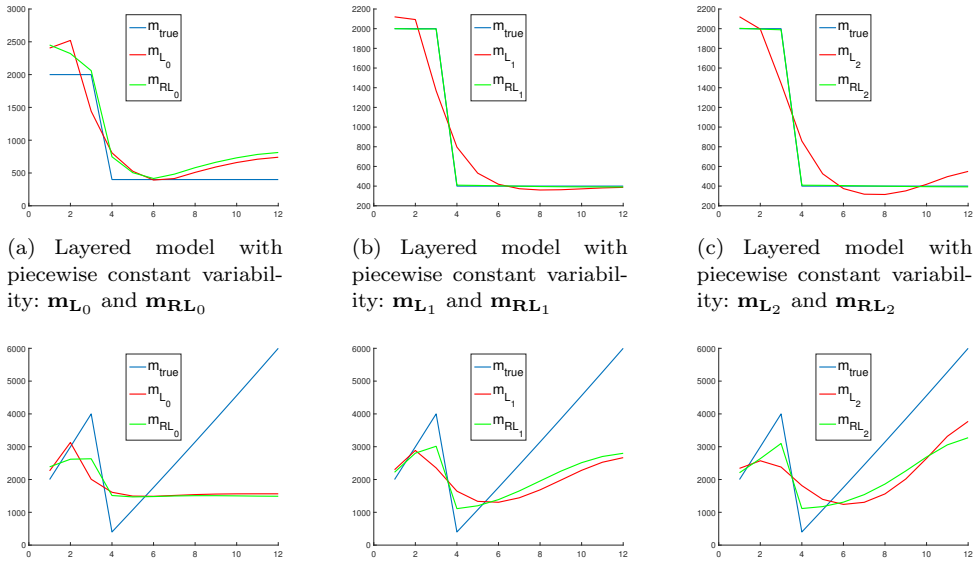

(a) Layered model with piecewise constant variability: $\mathbf{m_{L_0}}$ and $\mathbf{m_{RL_0}}$

(b) Layered model with piecewise constant variability: $\mathbf{m_{L_1}}$ and $\mathbf{m_{RL_1}}$

(c) Layered model with piecewise constant variability: $\mathbf{m_{L_2}}$ and $\mathbf{m_{RL_2}}$

(d) Layered model with strong linear variability: $\mathbf{m_{L_0}}$ and $\mathbf{m_{RL_0}}$

(e) Layered model with strong linear variability: $\mathbf{m_{L_1}}$ and $\mathbf{m_{RL_1}}$

(f) Layered model with strong linear variability: $\mathbf{m_{L_2}}$ and $\mathbf{m_{RL_2}}$

Figure 13. Average vertical resistivity of inverted models

The two-layered models in Figure 7 contain subregions distant from observations recorded at the surface that range in sensitivty. The inverted results are provided in Figures 10 - 12. Figure 10 is the simplest of the three models and we see that the standard 0^{th}, 1^{st}, and 2^{nd} derivative constraints exhibit significant smearing indicated by the red lines in Figures 10 (a)-(c). With knowledge of the boundary location at 7m depth, the discontinuous 1^{st} and 2^{nd} derivative constraints provide a more accurate representation of the true model, whereas the 0^{th} derivative constraint does not. The excellent quality of the reconstruction with the 1^{st} and 2^{nd} derivative constraints may be due to the inverse crime we have committed where the simulated data are on the same grid as the inverted results. Therefore, we ran the synthetic experiment with data generated on a different grid than the inversion. The data grid had a fixed height of 1 meter while the model grid starts at 1.75 meters at the surface and increases with depth. The results are in Figure 11 and are similar to those in Figures 10(b),(c),(e) and (f). In particular we see that including boundary information with 1^{st} and 2^{nd} derivative constraints still results in a superior inverted result, and therefore addresses

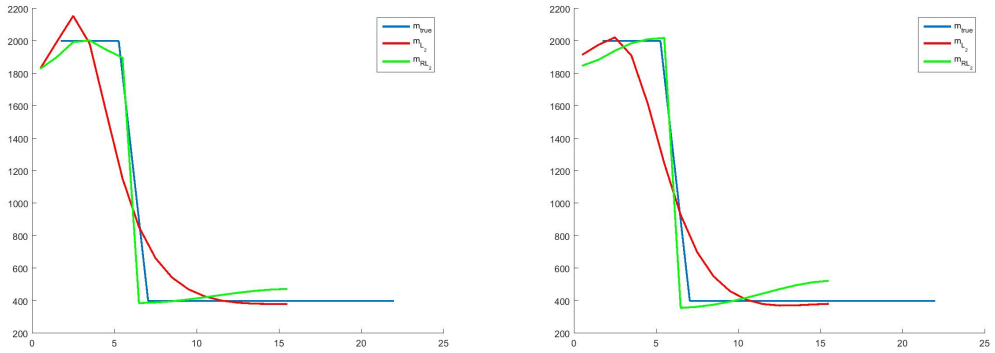

(a) Layered model with piecewise constant variability: $\mathbf{m_{L_1}}$ and $\mathbf{m_{RL_1}}$

(b) Layered model with piecewise constant variability: $\mathbf{m_{L_2}}$ and $\mathbf{m_{RL_2}}$

Figure 14. Average vertical resistivity of inverted models with data and inversion different grids.

the noise amplification of the data due to the ill-posedness of the problem.

Regardless of whether the data are generated on the same or different grid than the inverted results, we note that prior boundary knowledge incorporated as an initial parameter estimate gives significantly worse results than regularization with $\mathbf{RL}_1$ and $\mathbf{RL}_2$. This point is counter to most approaches where derivate constraints are used to smooth solutions, not to reconstruct discontinuities. It is also consistent with results in Section 2.3 for the idealized canonical model. Therefore, we focus on the ability of the regularization operator $\mathbf{R}$ to delineate different subregions with 1^{st} and 2^{nd} derivative constraints. These results can be observed more clearly through vertical slices representing the average horizontal resistivity with depth, provided in Figures 13 (a)-(c). These Figures show the smearing located near the discontinuity that takes place with standard regularization, whereas the additional regularization operator is able to capture the discontinuity. We see in Figure 14 that these conclusions still hold when the data are generated on a different grid than the inversion.

Two different amounts of linear variability were added to the two layered model which we call moderate and strong linear variability and are plotted in Figures 7 (b)-(c). The inverted results with the moderate variability model are similar to those with piecewise constant variability and so we omit the results. Inverted results in Figure 12 with strong variability show smearing so severe in the standard inversions that it is difficult to delineate the location of the discontinuity or detect the presence of linear variability. When the discontinuity is implemented with the 1^{st} and 2^{nd} derivative constraints operator, linearity is clearly observed within the upper subregion. However, inspection of vertical slices in Figures 13 (d)-(f) show a lack of linear variability in the lower subregion for all inverted types relative to the true model. This is likely due to a lack of sensitivity in the data, which implies that the degree of variability could limit the performance of the regularization operator. In these inverted results we find that $\mathbf{m}_{RL_2}$ performed the best and $\mathbf{m}_{RL_0}$ performed the worst. This difference in performance is evident in both subregions, where $\mathbf{m}_{RL_2}$ produced the most accurate amount of linearity relative to the true model.

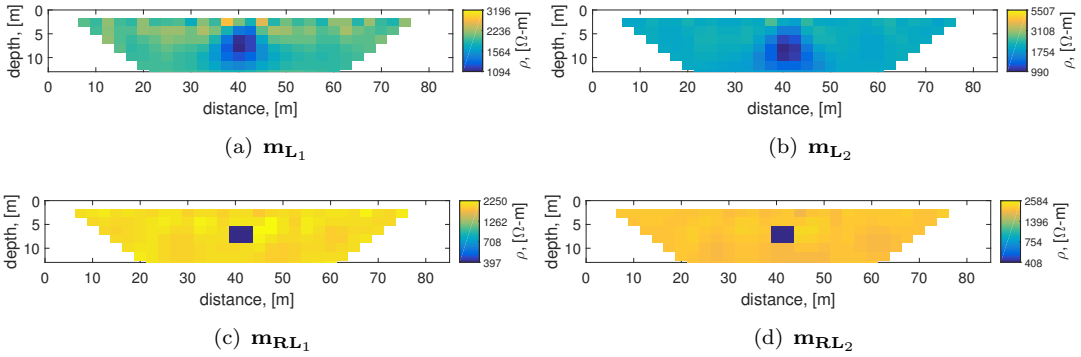

(a) $\mathbf{m_{L_1}}$ (b) $\mathbf{m_{L_2}}$

(c) $\mathbf{m_{RL_1}}$ (d) $\mathbf{m_{RL_2}}$

Figure 15. Inverted resistivity values for an anomaly model with piecewiseconstant variability.

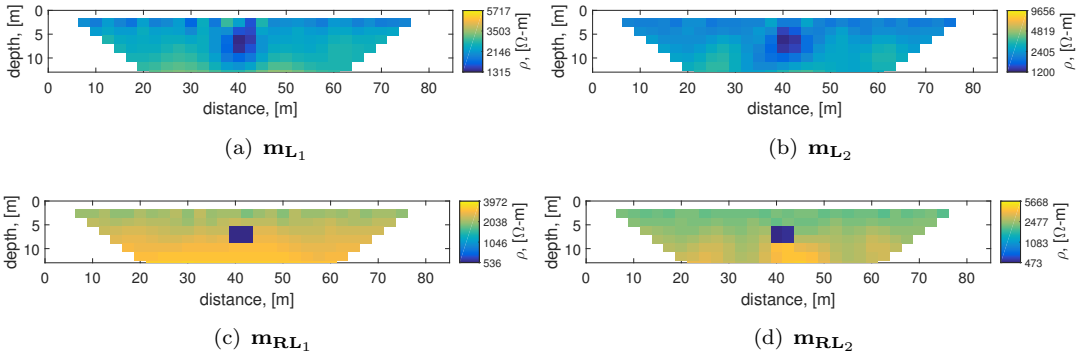

(a) $\mathbf{m_{L_1}}$ (b) $\mathbf{m_{L_2}}$

(c) $\mathbf{m_{RL_1}}$ (d) $\mathbf{m_{RL_2}}$

Figure 16. Inverted resistivity values for anomaly model with moderate linear variability

4.2.2. Anomaly Models

The anomaly models in Figure 8 contain a less sensitive subregion that covers a small area relative to the rest of the model. The inverted results in Figure 15 (a)-(b) show the continued pattern of smearing produced from standard inversions, whereas the incorporation of the proper boundary significantly improves this effect as seen in Figures 15 (c)-(d). The vertical slices in Figures 17 (a)-(b) show a drastic improvement in performance with the implementation of the regularization operator when compared to the standard inverted results. These Figures also show that the $\mathbf{RL}_1$ constraint produced a better result than the $\mathbf{RL}_2$ constraint, which produced artificial linear variability in the region below the anomaly.

The inverted results from the anomaly model with moderate linear variability are provided in Figure 16. The standard inverted parameters show the same smearing pattern, although both 1^{st} and 2^{nd} derivative constraints are able to produce some degree of linearity reflected in the true model. However, when the boundary location is provided in the inversion, smearing is greatly reduced and the degree of linearity has a stronger presence. The sensitivity to linearity is more clearly seen in the vertical slices provided in Figures 17 (c)-(d). These results show that the standard inversions indeed recover a significant amount of the linear variability, however the degree of accuracy is not as significant when compared to the results produced from the incorporation of the discontinuity. These results also show that $\mathbf{m}_{RL_1}$ performed slightly better than $\mathbf{m}_{RL_2}$ particularly in the region just below the anomaly.

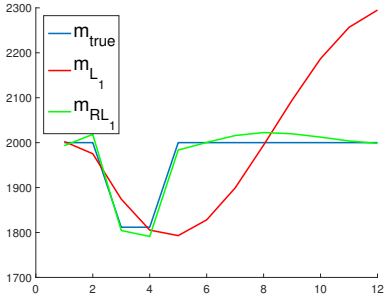

(a) Anomaly model with piecewise constant variability: $\mathbf{m_{L_1}}$ and $\mathbf{m_{RL_1}}$

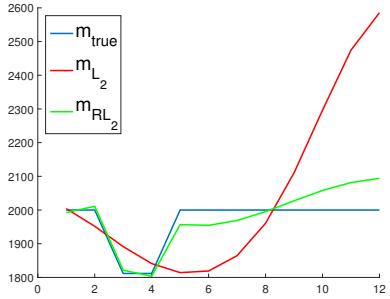

(b) Anomaly model with piecewise constant variability: $\mathbf{m_{L_2}}$ and $\mathbf{m_{RL_2}}$

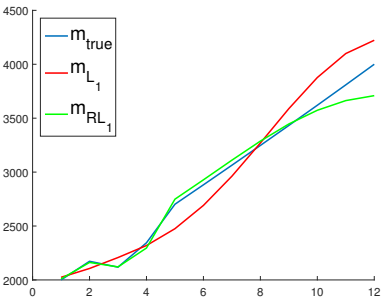

(c) Anomaly model with linear variability: $\mathbf{m_{L_1}}$ and $\mathbf{m_{RL_1}}$

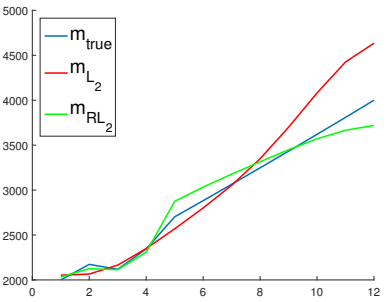

(d) Anomaly model with linear variability: $\mathbf{m_{L_2}}$ and $\mathbf{m_{RL_2}}$

Figure 17. Average vertical resistivity of inverted models

4.2.3. Sinusoidal Models

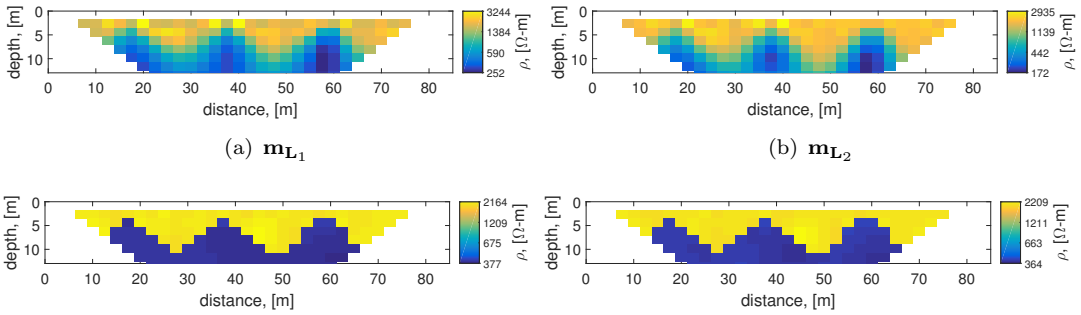

(a) $\mathbf{m_{L_1}}$ (b) $\mathbf{m_{L_2}}$

(c) $\mathbf{m_{RL_1}}$ (d) $\mathbf{m_{RL_2}}$

Figure 18. Inverted resistivity values for sinusoidal model with piecewise constant variability

The primary challenge with the sinusoidal models is the presence of a complex boundary geometry. The standard inversions in Figures 18 show the continued presence of smeared results and can only provide a general interpretation of the true model. However, the inverted results that contain the proper discontinuity removed a large degree of smearing. This is true for both 1^{st} and 2^{nd} derivative constraints, where the degree to which they converged to the true model is comparable. When moderate linear variability is introduced, the results in Figure 19 show significant improvement when the location of the discontinuity is incorporated in the inversion. Not only is a significant amount of smearing present in the standard inversions, but there is no clear

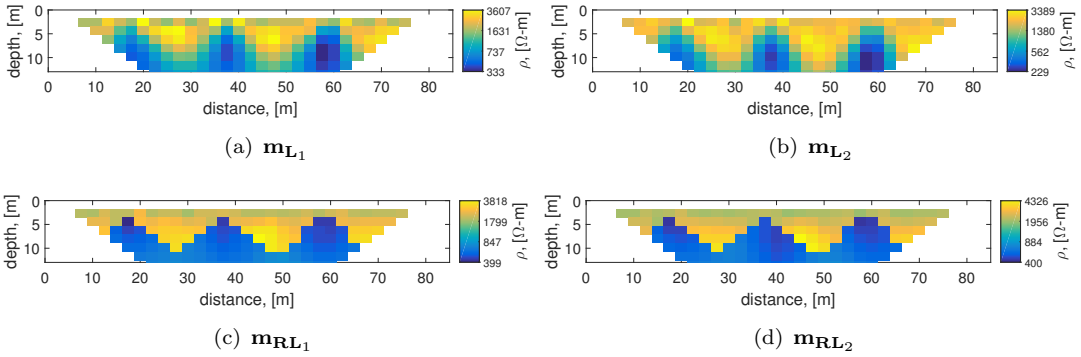

(a) $\mathbf{m}_{\mathbf{L}_1}$ (b) $\mathbf{m}_{\mathbf{L}_2}$

(c) $\mathbf{m}_{\mathbf{RL}_1}$ (d) $\mathbf{m}_{\mathbf{RL}_2}$

Figure 19. Inverted resistivity values for sinusoidal model with linear variability

indication of linear variability in the subregions. The discontinuous inversions recover most of the linear variability, particularly in the upper subregion. In these results, we see that the $\mathbf{RL}_2$ constraint performed better than the $\mathbf{RL}_1$ constraint, because it was able to capture the linear variability.

5. Discussion

These results show that the implementation of known discontinuities in the inversion process as described in Section 2 is likely to yield more optimal results, regardless of partial sensitivity between the observational data and subregions within the model parameters due to either subregions being far away from the observations, subregions with a small area of extent, or even a complex boundary geometry. The results also show how data sensitivity can limit the performance of implementing discontinuities in an inversion. We observed this in the two-layered model with a high degree of linear variability, where a bias is present in the lower subregion even with the implementation of the $\mathbf{RL}_2$ constraint term (Figure 13 (f)).

These results also show that incorporating discontinuity information with a 1^{st} or 2^{nd} derivative constraint is superior to incorporating the information with a 0^{th} derivative constraint. While $\mathbf{m}_{RL_0}$ performed better than $\mathbf{m}_{L_0}$, the 1^{st} or 2^{nd} constraint results $\mathbf{m}_{RL_1}$ and $\mathbf{m}_{RL_2}$ showed large performance gains relative to $\mathbf{m}_{RL_0}$. In order for the 0^{th} derivative constraint to effectively incorporate boundary information, the initial parameter estimate must be very accurate, which is not practical. Alternatively, incorporating boundary information with a 1^{st} or 2^{nd} derivate constraint only requires the location of the boundary, and not initial parameter value estimates.

We also found a small degree of variability between the performance of the 1^{st} and 2^{nd} derivative constraints. The 1^{st} derivative constrained inversions performed better where the true models had little variability within each subregion, whereas the 2^{nd} derivative constrained inversions performed better where the true models had significant linear variability. This is consistent with the canonical examples in Section 2.3. The primary difference between the canonical examples and the synthetic results is the degree of sensitivity, where the sensitivity was ideal in the canonical example, and lesser in the synthetic results. In fact, we suggest that this partial sensitivity explains why certain models, such as the two-layered model with piecewise constant variability had 2^{nd} derivative constraint results with linear variability even though the true model had only piecewise constant variability within each subregion.

6. Conclusions and Future Work

Tikhonov regularization with first and second derivative constraints is typically used to produces smooth inverse estimates [2]. This work explains how to produce discontinuous estimates with Tikhonov regularization through a diagonal regularization operator $\mathbf{R}$ with ones everywhere except at locations representing a discontinuity. Multiplying the regularization term by $\mathbf{R}$ removes the influence of the constraint on targeted regions for one dimensional problems and we extended the approach to two dimensions. In particular, we show how to identify the location of boundaries through 1^{st} and 2^{nd} derivative constraints. Moreover, we explain why boundary locations should be identified through first and derivative constraints and not included as prior knowledge in an initial parameter estimate.

An understanding of the influence of $\mathbf{R}$ on the regularization term gives insight to the effect of regularizing with a first derivative ($\mathbf{L}_1$) or second derivative ($\mathbf{L}_2$) constraint. We firstly noted that $\mathbf{L}_1$ and $\mathbf{L}_2$ regularization are more practical than $\mathbf{L}_0$ for discontinuous inversions since they require less prior information. Secondly we found that the $\mathbf{L}_1$ constraint is the best choice when the true model contains constant variability in subregions. Alternatively, if there is linear variability in subregions the $\mathbf{L}_2$ constraint is optimal. In particular, we showed that if there is a lack of sensitivity between the observations and particular subregions, then $\mathbf{L}_1$ will necessarily produce piecewise constant variability while $\mathbf{L}_2$ will produce linear variability in the subregions.

We have provided an in depth analysis of the incorporation of sharp discontinuities with least squares so that it can be applied to more practical problems. It may be counter intuitive to use least squares for sharp discontinuities. However, by incorporating a matrix $\mathbf{R}$, piecewise, continuous results are obtained and hence we have shown exactly how least squares can most effectively capture discontinuities. When dealing with real data where prior knowledge is not perfectly known (i.e. the location of a boundary), more elaborate techniques are required to appropriately weight such prior information. This is typically accomplished by a covariance matrix that acts on the constraint in the regularization term. For example, it has been shown that the covariance matrix can be formed from variogram estimates of the model parameters [14]. However, this approach finds a covariance matrix for the 0^{th} derivative of the model parameters. We have shown it is more advantageous to use 1^{st} and 2^{nd} derivative constraints for problems with discontinuities. Therefore, a more appropriate implementation in this setting would be to construct a variogram of the 1^{st} or 2^{nd} derivative of the model parameters. This will be the focus of future work, where we incorporate inexact boundaries with real data.

Funding

This work was supported by the National Science Foundation under grant number DMS-1418714.

References

[1] Adler A and Lionheart WR. Uses and abuses of EIDORS: an extensible software base for EIT. Physiological measurement. 2006;27(5):S25.

[2] Aster RC, Borchers B, Thurber CH. Parameter estimation and inverse problems. 2nd ed. Elsevier Academic Press; 2013.
[3] Alberti GS, Ammari H, Jin B, Seo JK, and Zhang W. The linearized inverse problem in multifrequency electrical impedance tomography. SIAM J. Imaging Sci. 2016;9(4):1525–1551.
[4] Ammari H, Kwon O, Seo JK, and Woo EJ. T-Scan electrical impedance imaging system for anomaly detection. SIAM J. Appl. Math.2004;65(1):252–266.
[5] Binley A, Cassiani G, Middleton R, et al. Vadose zone flow model parameterisation using cross-borehole radar and resistivity imaging. Journal of Hydrology. 2002;267:147–159.
[6] Zonge K, Wynn J, Urquhart S. 9. resistivity, induced polarization, and complex resistivity; 2005. Chapter 9; p. 265–300. Available from: http://library.seg.org/doi/abs/10.1190/1.9781560801719.ch9.
[7] Constable S, Parker RL, Constable CG. Occams inversion: a practical algorithm for generating smooth models from electromagnetic sounding data. Geophysics. 1987;52(3):289–300.
[8] Daily W, Ramirez A, Labrecque D, et al. Electrical resistivity tomography of vadose water-movement. Water Resources Research. 1992;28:1429–1442.
[9] deGroot Hedlin C, Constable S. Occams inversion to generate smooth, two dimensional models from magnetotelluric data. Geophysics. 1990;55:1613–1624.
[10] Doetsch J, Linde N, Pessognelli M, et al. Constraining 3-d electrical resistance tomography with gpr reflection data for improved aquifer characterization. Journal of Applied Geophysics. 2012;78:68–76.
[11] Doetsch J, Linde N, Binley A. Structural joint inversion of timelapse crosshole ert and gpr traveltime data. Geophysical Research Letters. 2010;37.
[12] Günther T, Rücker C. A general approach for introducing information into inversion and examples from dc resistivity inversion; 2006. 10th Annual European Meeting of Environmental and Engineering Geophysics, EAGE. Extended Abstract.
[13] Henderson RD, Day-Lewis FD, Abarca E, et al. Marine electrical resistivity imaging of submarine groundwater discharge: Sensitivity analysis and application in waquoit bay, massachusetts, usa. Hydrogeology Journal. 2010;18:173–185.
[14] Hermans T, Vandenbohede A, Lebbe L, et al. Imaging artificial salt water infiltration using electrical resistivity tomography constrained by geostatistical data. Journal of Hydrology. 2012;438-439:168–180.
[15] Johnson TC, Versteeg RJ, Rockhold M, et al. Characterization of a contaminated wellfield using 3d electrical resistivity tomography implemented with geostatistical, discontinuous boundary, and known conductivity constraints. Geophysics. 2012;77(6):85–96.
[16] Kaipio JP, Kolehmainen V, Vauhkonen M and Somersalo E. Inverse problems with structural prior information. Inverse problems. 1999;15(3):713.
[17] Karaoulis M., Tsourlos P, Kim JH and Revil A. 4D time-lapse ERT inversion: introducing combined time and space constraints. Near Surface Geophysics. 2014;12(1):25–34.
[18] Kemna A, Vanderborght J, Kulessa B, et al. Imaging and characterization of subsurface solute transport using electrical resistivity tomography (ert) and equivalent transport models. Journal of Hydrology. 2002;267:125–146.
[19] Key K. 1d inversion of multicomponent, multifrequency marine csem data: Methodology and synthetic studies for resolving thin resistive layers. Geophysics. 2009;74(2).
[20] Mead J. Discontinuous parameter estimates with least squares estimators. Applied Mathematics and Computation. 2013;219:5210–5223.
[21] Mead JL, Renaut RA. A newton root-finding algorithm for estimating the regularization parameter for solving ill-conditioned least squares problems. Inverse Problems. 2009;25(2).
[22] Mead JL. Parameter estimation: A new approach to weighting a priori information. Journal of Inverse and Ill-posed Problems. 2008;16(2):175–194.
[23] Miller CR, Routh P, Brosten T, et al. Application of time-lapse ert to watershed characterization. Geophysics. 2008;73.
[24] Muller K, Vanderborght J, Englert A, et al. Imaging and characterization of solute trans-

port during two tracer tests in a shallow aquifer using electrical resistivity tomography and multilevel groundwater samplers. Water Resources Research. 2010;46.
[25] Pidlisecky A, Knight R. Fw25d: A matlab 2.5d electrical resistivity modeling code. Computers and Geosciences. 2008;34(12):1645–1654.
[26] Saunders JH, Herwanger J, Pain CC, et al. Constrained resistivity inversion using seismic data. Geophysical Journal International. 2005;160:785–796.
[27] Slater LD, Sandberg SK. Resistivity and induced polarization monitoring of salt transport under natural hydraulic gradients. Geophysics. 2000;65:408420.
[28] Slater LD, Binley A. Synthetic and field-based electrical imaging of a zerovalent iron barrier: Implications for monitoring long-term barrier performance. Geophysics. 2006; 71(5):129137.
[29] Toto EA, Basri ME, Al-Hajari SA, et al. Karst and saltwater intrusion mapping using electric resistivity tomography: Case study at the site of cap rhir, southern morocco. Near Surface Geophysics. 2008;6:321–329.
[30] Smith T, Hoversten M, Gasperikova E, et al. Sharp boundary inversion of 2d magnetotelluric data. Geophysical Prospecting. 1999;47:469–486.
[31] Ward AS, Gooseff MN, Singha K. Imaging hyporheic zone solute transport using electrical resistivity. Hydrological Processes. 2010;24(7).